



Microstructural, optical, and electrical characteristics of Cu-doped CdTe nanocrystalline films for designing absorber layer in solar cell applications

Meshal Alzaid^{1,*}, N. M. A. Hadia^{1,2}, M. El-Hagary³, E. R. Shaaban⁴, and W. S. Mohamed^{1,2,*} 

¹ Physics Department, College of Science, Jouf University, P.O. Box: 2014, Sakaka, Saudi Arabia

² Physics Department, Faculty of Science, Sohag University, Sohag 82524, Egypt

³ Physics Department, Faculty of Science, Helwan University, Helwan 11792, Cairo, Egypt

⁴ Physics Department, Faculty of Science, Al-Azhar University, Asyut, Egypt

Received: 11 March 2021

Accepted: 26 April 2021

Published online:
20 May 2021

© The Author(s), under exclusive licence to Springer Science+Business Media, LLC, part of Springer Nature 2021

ABSTRACT

This paper reports the microstructure, optical, and electrical characteristics of undoped and Cu-doped CdTe nanostructured thin films prepared on glass substrates by electron beam evaporation technique. The crystallographic study of X-ray diffraction shows that CdTe and Cu-doped CdTe films crystallize in the form of a cubic zinc blende structure. Microstructure analysis reveals that as the Cu-doping level increases, the average crystallite size increases, while the microstrain decreases due to the improvement of the crystallinity, thereby reducing defects. XRD and AFM investigations confirmed the nanostructure characteristic of undoped and Cu-doped films. It was found that the optical band gap energy increases from 1.485 to 1.683 eV as the Cu concentration increases from 0 to 10 wt%, which may be related to the Burstein–Moss effect. The refractive index is calculated from the Swanepoel envelope method and found to decrease with the increase of the Cu doping due to the decrease in the polarizability. Similarly, the extinction coefficient decreases with the increase of Cu in the CdTe matrix. The dc electrical conductivity is found to increase with increasing Cu doping, which is attributed to the increase in the grain size, thereby reducing the scattering of the grain boundary. Furthermore, two conduction mechanisms of the carrier transport in nanostructured undoped and Cu-doped CdTe films were observed. The low-temperature dependence of the conductivity of undoped and Cu-doped CdTe nanostructured films is explained based on Mott's variable range hopping conduction mechanism model (VRH). Interestingly, the calculated values of hopping distance R , the hopping energy W , and the density of states at the Fermi level $N(E_F)$ are consistent with Mott's VRH. Finally, Hall effect measurements show that all the films have p-type conduction behavior. Besides, the results show that as the Cu doping level

Address correspondence to E-mail: mmalzaid@ju.edu.sa; wael-saad@science.sohag.edu.eg

increases, the carrier concentration and the Hall mobility increase due to the decrease in grain boundary scattering with the increase in grain size. Accordingly, it can be concluded that by increasing the Cu doping level in the CdTe film, the conductivity is increased, thereby improving the performance of the CdTe absorber layer in the solar cell structure.

1 Introduction

In recent years, the binary semiconductor compounds $A^{II}B^{VI}$ are provided a great deal of interest due to their potential application in solar cells and photoconductive devices [1]. Cadmium telluride (CdTe) is a member of the $A^{II}B^{VI}$ semiconductor compound family, which is considered to be one of the most outstanding absorber layers for solar cells because of its unique characteristics, such as direct band gap (1.5 eV) at room temperature located in the central spectrum of the solar spectrum, highly absorption coefficient in the visible region of the solar spectrum ($\alpha \approx 10^5 \text{ cm}^{-1}$) [2], good transport performance, high average atomic number (50), high resistivity, and exhibiting n-type and p-type conductivity, which allows the production of solar cells with heterojunction and homojunction structure [3]. CdTe has a sharp absorption edge, which allows 90% of incident photons to be absorbed in a 2- μm opaque CdTe layer, whereas the absorption of similar radiation intensity needs thick layer of 20 μm in the case of Si [4]. All these characteristics make CdTe an ideal candidate materials for various applications, e.g., photovoltaic conversion, solar cell structure, field effect transistors, and X-ray and gamma-ray detectors (role [5, 6]). Several deposition techniques have been used to fabricate CdTe thin films, such as RF sputtering [7], chemical bath deposition [8], pulsed laser deposition [9], close-range sublimation [10], electrodeposition [11], thermal evaporation [12], and electron beam evaporation [13]. Nevertheless, the difficult duty is to obtain stoichiometric CdTe films to better design the absorber layer in the solar cell structure, since defects and/or impurities generated during the deposition process will affect the optoelectronic properties of prepared thin films, thereby changing the efficiency of the solar cells [14–17]. Also, it is reported that the electrical and optical properties of CdTe thin films are tuned by doping with an appropriate dopant (Bi, Co, Ag, Cu, In, and Mo) into CdTe semiconductor lattice, which enhances the

efficiency of solar cells [18–23]. In this context, Cu was reported to be an amphoteric dopant type, that can be involved in the CdTe lattice as an interstitial ion (Cu_i^+), producing a shallow donor level, or substituted by Cd atoms to form a deeper acceptor level (Cu_{Cd}^-), or complexes contain Cu^+ and Cd vacancies ($\text{Cu}_i^+ + \text{V}_{\text{Cd}}^{-2}$) and ($\text{Cu}^+ - \text{Cu}_{\text{Cd}}$), forming shallow acceptors [24]. One of the main advantages of Cu doping into CdTe is the increase in carrier concentration, which can improve the ohmic contact.

In this paper, the electron beam evaporation technique is used to deposit high-quality undoped and Cu-doped CdTe nanocrystalline thin films with different Cu concentrations on glass substrates. The detailed analysis of the microstructure, morphology, optical, and electrical properties of CdTe and Cu-doped CdTe nanocrystalline films is studied, which is very important for the design of the absorber layer in the solar cell structure.

2 Materials and methods

CdTe and Cu-doped CdTe ingots with different Cu concentrations (0, 2, 4, 6, 8, and 10 wt%) have been synthesized using the mechanical milling method. Analytical grades with stoichiometric CdTe and Cu_2Te powders (with a chemical purity of 99.999%, Aldrich) were mixed and milled in a mechanical ball mill machine at 200 rpm for 6 h. The mixture is made disk shaped to avoid splashing the mixture powders during the evaporation process. The prepared pure and Cu-doped CdTe ingots were used as a source for thin film deposition. The CdTe and Cu-doped CdTe thin films with various Cu concentrations were deposited by electron beam evaporation technique (Edward Auto 306) at room temperature. Amorphous glass with a size of (25 mm \times 25 mm) is used as the substrate. To clean the substrate carefully, the substrate was immersed in acetone for 15 min and then washed with purified water for 15 min, and subsequently with alcohol for 10 min. At last, the substrate

was ultrasonically cleaned in deionized water for 15 min and then was dried in air at a temperature of 100 °C. The substrates and ingots have been placed in the chamber, which was then evacuated at the pressure of 5×10^{-6} Pa. The pellet ingot was preheated for 5 min before evaporation to remove any pollutants and degas the pellets. The distance from the substrate to the source is kept at about 20 cm. The thickness of the film was adjusted at 300 nm at a deposition rate of 2 nm/sec, which was controlled by a thickness monitor device (model; FTM6). More details of the deposition methodology are explained elsewhere [25].

X-ray diffractometer (XRD, Cu-K α = 1.54056 Å, Philips diffraction 1710) was used for crystallographic investigation. The ratio of the elemental composition of the film was checked by using energy-dispersive X-ray spectroscopy (EDXS). The surface morphology of the film was performed using an atomic force microscope (AFM, model MLCT-MT-A). The transmission and reflection spectra were measured with a dual-beam spectrophotometer (UV-Vis-NIR, Shimadzu model V-670). The electrical performance was studied by using the Hall measurement technique in van der Pauw configuration with a 0.6 T magnetic field (model Ecopia-HMS-3000).

3 Results and discussion

3.1 Elemental composition analysis

The elemental composition analysis of Cu-doped films with different Cu doping levels has been performed by EDXS measurements. The quantitative weight percentage of the elemental composition is

Table 1 The quantitative weight percentage of the elemental composition of the as-deposited nanostructured Cu doped CdTe films from EDXS analysis

Compound	wt%		
	Cd	Cu	Te
CdTe: Cu 0 wt%	48.42	–	51.58
CdTe: Cu 2 wt%	47.91	2.09	50.70
CdTe: Cu 4 wt%	46.72	3.88	50.80
CdTe: Cu 6 wt%	43.89	6.07	50.04
CdTe: Cu 8 wt%	40.98	8.11	50.91
CdTe: Cu 10 wt%	39.07	10.04	50.89

given in Table 1. The results show that the calculated weight percentage of the Cd, Te, and Cu elements are close to the nominal stoichiometry within the experimental error range. Besides, the data further reveal that nominal Cu content increases with the increase of Cu doping. This specifies that the Cu ions have successfully incorporated into the CdTe matrix and replaced Cd ions, thus verifying the conclusion of XRD results.

3.2 Structural and microstructure characterizations

Figure 1a shows the XRD patterns of undoped and Cu-doped CdTe (CdTe: Cu) thin films deposited by electron beam evaporation method at room temperature on a glass substrate with different Cu concentrations of 2, 4, 6, 8, and 10 wt%. The results reveal that all films have a polycrystalline-like structure with three reflection lines belonging to (111), (220), and (311) diffraction planes of cubic zinc blende structure suggested the existence of the cubic phase of CdTe structure (JCPDS No. 01-075-2086). Also, the XRD patterns reveal a preferred oriented grain growth toward the (111) plane due to the challenge between the energy of surface and strain energy [26]. It is worth noting that the XRD patterns did not show any foreign peak related to copper phases, such as copper oxide and or copper cluster, indicating a successful inclusion of Cu²⁺ ions into the CdTe lattice without change of cubic structure of CdTe. It was found from Fig. 1b that the peak position of the (111) plane is shifted toward higher diffraction angles due to the strain in the film by the incorporation of Cu ions in the CdTe structure of the semiconductor matrix with remarkable shrinks in the cell volume. Figure 2a shows the reduction of the lattice parameter (*a*) with increasing Cu incorporation into CdTe host lattice, which is calculated from interspacing planner distance (*d*) and lattice indices (*hkl*) of the most predominantly preferred oriented peak by using the standard equation of cubic structure: $\frac{1}{d_{hkl}^2} = (h^2 + k^2 + l^2)/a^2$. The observed reduction of the lattice parameter is attributed to the incorporation of Cu²⁺ ions of smaller ionic radius (0.72 Å) by Cd²⁺ ions of larger ionic radius (0.97 Å). The calculated value of the lattice parameter of Cu doped film with different Cu doping levels is provided in Table 2. As can be observed, the obtained lattice parameter (*a*)

Fig. 1 **a** XRD diagrams of undoped and Cu doped thin films at Cu concentrations, **b** The magnification of diffraction peak at (111) plane

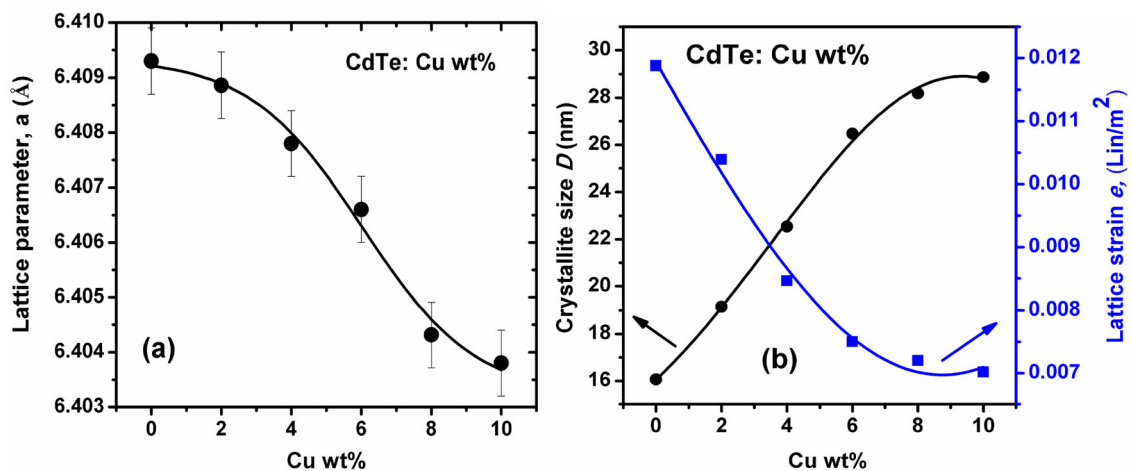
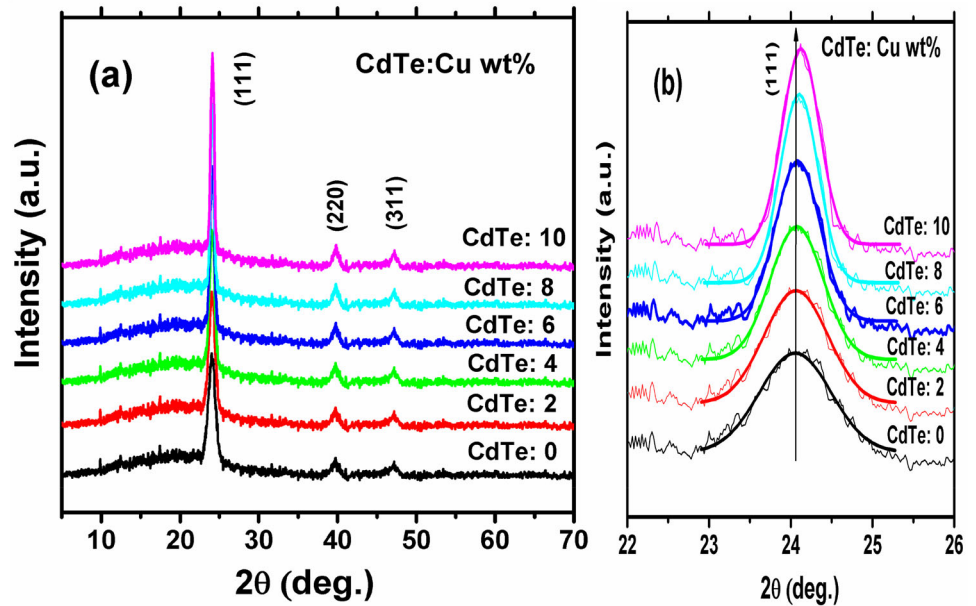


Fig. 2 **a** The lattice parameter versus Cu concentration in CdTe matrix. **b** The variation of the microstructural parameters with different Cu concentrations of undoped and Cu doped CdTe films

Table 2 Structural and microstructural properties of undoped and Cu doped CdTe thin films

CdTe: Cu (wt%)	a (Å)	V (Å) ³	Average crystallite size obtained from XRD (nm)	$e \times 10^{-3}$ (Lin m ⁻²)	Average grain size obtained from AFM (nm)	Surface roughness (nm)	RMS surface roughness (nm)
0	6.4093	263.29	16.07	1.19	28.61	2.446	2.283
2	6.4089	263.23	19.15	1.04	34.34	2.102	2.112
4	6.4078	263.10	22.54	0.85	41.12	1.283	1.113
6	6.4066	262.95	26.47	0.75	43.56	1.134	1.072
8	6.4043	262.67	28.18	0.72	49.56	0.812	0.623
10	6.4038	262.61	28.87	0.70	56.23	0.622	0.420

value of undoped CdTe is consistent with the standard value of CdTe cubic structure (6.41 Å, JCPDS No. 01-075-2086). Furthermore, the intensity of the preferred oriented peak (111) is improved and its full width at half maximum of diffraction peak (FWHM) decreases with the increase of the Cu doping, which is attributed to the improvement of the crystal growth of the film due to the occupation of Cd site by Cu ions. This behavior was given in the literature for Mo doped CdTe [24] and Cu doped CdTe thin films [27]. Besides, the nanostructure nature of the films is examined by using Debye–Scherrer's equations from the calculations of the mean crystallite sizes, $D = \frac{k\lambda}{\beta \cos \theta}$ and lattice microstrain, $\varepsilon = \frac{\beta}{4 \tan \theta}$ where, θ , β , k , and λ are the Bragg angle of the most preferred oriented peak, radian FWHM, shape factor (≈ 0.9), and the wavelength of the CuK α radiation, respectively. The value of the average crystallite size of the Cu doped CdTe film is found to vary from 16.07 nm for CdTe to 28.87 nm for CdTe: 10 wt%, confirming the nanostructure characteristic of the film. Figure 2b displays the dependence of the microstructure parameters with Cu doping, see also Table 2. It can be observed that as the Cu doping increases, the average crystallite size increases, while the microstrain decreases, which refers to the improvement of the crystallinity and the reduction of the defects due to the complete integration of Cu²⁺ ions into the CdTe lattice. Such an increase in the average crystallite size and decrease in microstrain is reported for films that have smaller ionic radius dopants [28].

3.3 Surface morphology analysis

The microscopic description of the surface morphology of the undoped and Cu-doped CdTe films has been performed using AFM investigation. Figure 3 shows the three-dimensional (3D) AFM images of CdTe, CdTe: 4 wt%, and CdTe: 10 wt% films. The images show that the surface of the films has a highly densely spherical elongated packing grain with a uniform arrangement. The observed regular distribution of the elongated spherical grains with similar directions confirms the observed preferred oriented grain growth toward the (111) plane. The micrographs of the CdTe and Cu-doped films were analyzed in detail to identify the microscopic surface morphology parameters, such as the grain size, surface roughness, and root mean square (RMS) surface

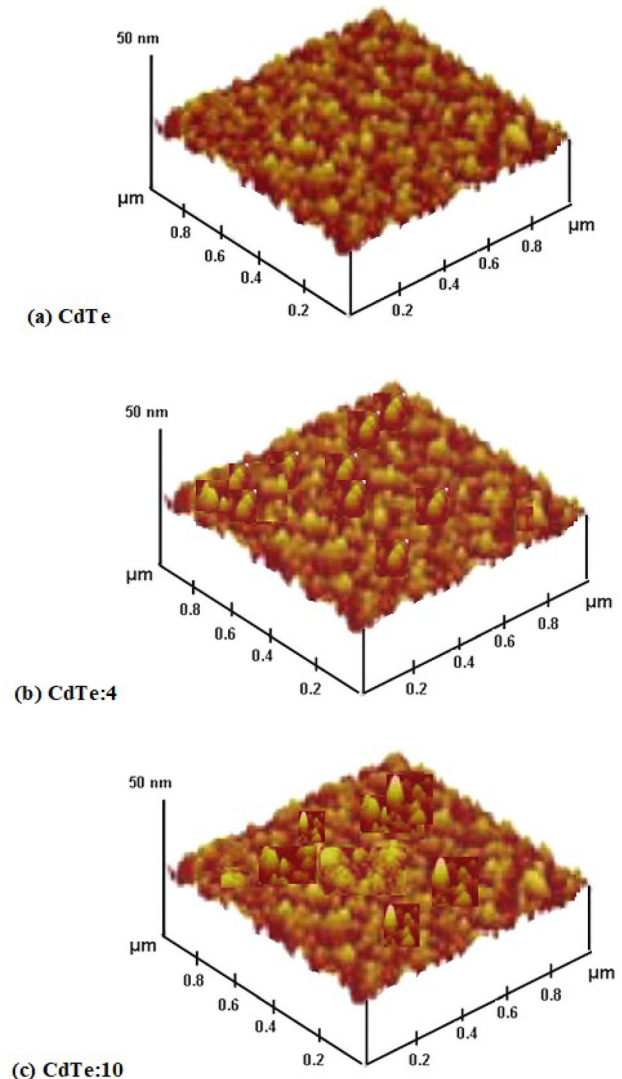


Fig. 3 3D AFM micrographs of Cu doped CdTe films

roughness, see Table 2. The data show that the grain size increases with the increase of the Cu concentration into CdTe lattice. However, it was found that the surface roughness and RMS surface roughness are decreased with the increase of the Cu doping. The reduction in the surface roughness with the increase of Cu doping into the CdTe films [27] and ZnO films [29] is reported in the literature. It has to be mentioned that the grain size obtained from SEM is higher than the crystallite size calculated by XRD. This inconsistency can be ascribed to the fact that the crystallite size is a record of the size coherent scattering domain, while the grain size is a set of this coherently scattering domain separated by a grain boundary. Besides, crystallite size reveals two distinct ranges when dislocations are located in the

composition, while the difference between them is not visible in the SEM micrographs [30].

3.4 Optical properties

The optical band gap energy of the semiconductor films is calculated from the absorption spectra of the films via their transmission and reflection measurements. Figure 4 shows the spectral dependence of transmittance T and reflectance R measurements of nanocrystalline Cu doped CdTe film with various Cu doping levels in the wavelength range 200–2500 nm. The average transmittance in the near-infrared region was found to vary from 78 to 82%. Thus, the highly transparent Cu-doped CdTe films can be used in n-type window layer for photovoltaic solar cell applications as reported for highly transmission CdS film [31, 32] and CdO [33] thin film. It is clearly observed that the transmittance reasonably increases with the increment of the Cu content into the CdTe host lattice which is attributed to the improvement of the crystallinity, see XRD analysis. The thickness uniformity and surface smoothness of the film can be verified by the appearance of interference fringes, which is due to the coherence of multiple transmitted lights at the interface between the film and substrate. Furthermore, the transmission curve drops sharply at the absorption edge due to the transition of an electron from the valence band (VBM) to the conduction band

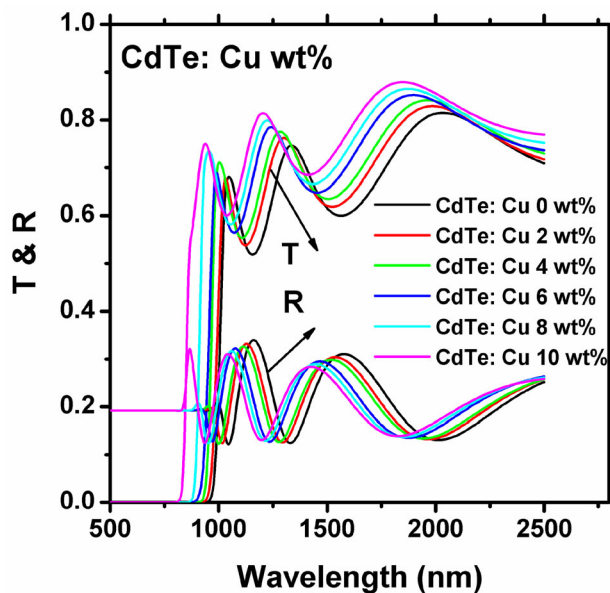


Fig. 4 The spectral variation of the transmittance and reflectance of pure and Cu-doped CdTe films with various Cu contents

(CBM). It is found further that as the concentration of Cu into CdTe increases, the absorption edge blue shifts, which indicates that the fundamental energy gap increases with the increase of Cu doping. Figure 5a depicts the absorption coefficient as a function in photon energy of nanostructured Cu-doped CdTe film with different Cu dopants, which are evaluated from the transmission and reflection measurements in the strong absorption region by using the following relation [34]:

$$\alpha(\lambda) = \left(\frac{1}{d}\right) \ln(X \times Y), \quad (1)$$

$$X = [(1 - R_1)(1 - R_2)(1 - R_3)]/[2T(1 - R_2R_3)], \quad (2)$$

and

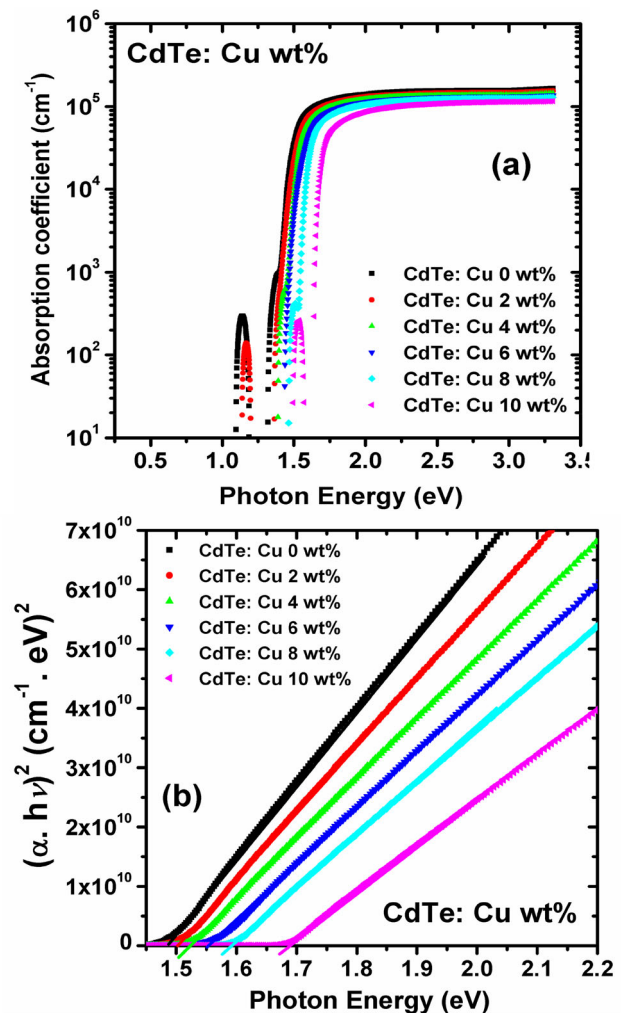


Fig. 5 a The absorption coefficient versus photon energy of pure and Cu-doped CdTe films at different Cu dopants b $(\alpha h\nu)^2$ versus $h\nu$ of undoped and Cu-doped CdTe films at different Cu contents

$$Y = 1 + \{1 + [R_1(R_2 + R_3 - 2R_2R_3)] / (1 - R_2R_3)A^2\}^{1/2}, \quad (3)$$

where d is film thickness, and R_1 , R_2 , and R_3 represent the power of Fresnel reflection coefficients for an air–film interface, for film–substrate interface, and for a substrate–air interface, respectively. The films show a high absorption coefficient value ($\approx 10^5 \text{ cm}^{-1}$), which can be used as an absorber layer in solar cells. The results reveal further that the absorption coefficient decreases with increasing copper concentration. Moreover, the absorption value suddenly decreases at the absorption edge, which is observed to shift to higher energy as the Cu incorporation level increases. The optical band gap energy of nanostructured Cu doped film with the variety of Cu contents is estimated using Tauc's model [35, 36]:

$$(\alpha h\nu)^{1/n} = \alpha_0(h\nu - E_g), \quad (4)$$

where α_0 is constant and the value of the exponent n represents the direct ($n = 1/2$) [37]. The Tauc's relation is represented in Fig. 5b by $(\alpha h\nu)^2$ versus $(h\nu)$. The linear part of Tauc's plot is extrapolated to $(\alpha h\nu)^2 = 0$. The optical band gap energy E_g^{opt} is determined from the intersection of the extrapolated line with $(\alpha h\nu)^2 = 0$. The obtained values of E_g^{opt} for nanocrystalline undoped and Cu doped CdTe film is provided in Table 3. Obviously, the optical band gap energy of undoped CdTe film ($E_g^{\text{opt}} = 1.485 \text{ eV}$) is in accordance with the published value ($E_g^{\text{opt}} \approx 1.49 \text{ eV}$) [1]. Moreover, it is observed that the optical band gap energy increases with the increase of Cu incorporation level in CdTe lattice, which may be related to the Burstein–Moss effect. This effect is corresponding to degenerate doping semiconductors, in which the Fermi level lies inside the conduction band. According to the Burstein–Moss effect, as the Cu incorporation increases into CdTe, the electron carrier density of states of the conduction band edge increases. Therefore, the energy band gap increases with increasing Cu incorporation level when the electrons are excited from the maximum edge of the valance band to the conduction band above the Fermi level since all the states below the Fermi level are occupied. This effect is also reported for the increase of energy band gap in Mo doped CdTe films [23] and Mo doped CdO films [38].

It is worth mentioning that the optical constants, such as the refractive index and extinction coefficient, of semiconducting materials are essential optoelectronic parameters for designing the solar cell and photovoltaic devices. The refractive index of semiconductor thin films was calculated with different methods [39–44]. In this context, the refractive index of nanostructured Cu doped CdTe thin film is calculated by using Swanepoel method [45], and then later improved by Manifacier et al. [46]. This method is based on the suppression of the observed interference patterns in the transmittance spectra by constructing envelope curves around maxima and minima transmittance. The detailed process of this method has been described elsewhere [47, 48]. The spectral variation of the refractive index of nanostructured Cu doped CdTe films is shown in Fig. 6a. The figure shows a normal dispersion behavior for the spectral variation of the refractive index of the undoped and Cu-doped CdTe nanostructured films. It is important to note that as the Cu-incorporation level increases, the overall behavior of the refractive index decreases. This decrease in refractive index is related to the observed increase in optical band gap energy with increasing Cu incorporation level, which is inversely correlated through different empirical models [49–51]. Lorentz–Lorenz equation relates the refractive index directly with the polarizability [52]. The substitution of Cd of larger atomic radius (1.61 Å) by Cu of smaller atomic radius (1.45 Å) raises the density and thus diminishes the polarizability.

Accordingly, the decrease in the refractive index with the increase of Cu incorporation level is due to the decrease in the polarizability. On the other hand, the increase of the crystallinity and the grain size of CdTe film with the increase of the Cu concentration may also be another reason for the decrease in refractive index [53]. The extinction coefficient (k) of CdTe and Cu-doped CdTe films is determined from the following equation $\alpha = 4\pi k/\lambda$ [54]. The spectral behavior of the excitation coefficient of undoped and Cu doped CdTe nanocrystalline films is displayed in Fig. 6b. It is can be observed that the extinction coefficient drastically dropped to the lowest value at the strong absorption region that is due to the total absorption of the incident photons at the fundamental absorption edge. The figure further shows that the overall extinction coefficient decreases with the increase of the Cu incorporation levels.

Table 3 The optical band gap energy and electrical properties of pure and Cu doped CdTe films

CdTe: Cu (wt%)	E_g^{opt} (eV)	E_{a1} (eV)	E_{a2} (eV)	300 K		μ_H $\text{cm}^2 \text{V}^{-1} \text{s}^{-1}$	$n_H \times 10^{18}$ (cm^{-3})	$T_o \times 10^5$ (K)	$N(E_F) \times 10^{17}$ ($\text{eV}^{-1} \text{cm}^{-3}$)	W (eV)	$R \times 10^{-4}$ (cm)	αR
				$\rho \times 10^4$ (Ωcm)	$\sigma_{dc} \times 10^{-6}$ ($\Omega^{-1} \text{cm}^{-1}$)							
0	1.485	0.578	0.058	66.5	1.50	13.05	7.2	33.82	1.178	0.053	5.923	734
2	1.508	0.429	0.047	18.1	5.52	37.55	9.2	17.30	2.302	0.045	3.03	375
4	1.523	0.424	0.034	8.90	10.23	58.65	11.9	6.75	5.899	0.036	1.183	146
6	1.565	0.354	0.028	4.10	24.39	69.63	21.9	4.09	9.738	0.031	0.716	88
8	1.601	0.342	0.026	2.60	38.46	78.74	30.4	3.36	11.833	0.03	0.589	73
10	1.683	0.306	0.025	2.20	45.54	83.19	33.8	2.78	14.279	0.029	0.489	60

3.5 Electrical properties

The room-temperature carrier concentration, carrier type, and carrier mobility of undoped and Cu-doped CdTe nanostructured films with different Cu concentrations were determined by Hall effect measurements. It can be observed that these films have p-type conduction behavior, which is determined by the sign of the positive Hall coefficient. Figure 7 depicts the room-temperature values of Hall mobility μ_H , carrier concentrations n_H , and resistivity ρ of nanostructured undoped and Cu-doped CdTe film with various Cu incorporation levels. The results show that as Cu increases from 0 to 10 wt%, the carrier concentration and the Hall mobility increase from $7.20 \times 10^{18} \text{ cm}^{-3}$ to $33.75 \times 10^{18} \text{ cm}^{-3}$ and from 14.08 to $83.19 \text{ cm}^2 \text{ V s}^{-1}$, respectively. The increase in Hall mobility and carrier concentration with Cu doping is attributed to the decrease in the scattering of the grain boundary, which is due to the increase in grain size originated with the rise in Cu doping level. This can be confirmed from AFM measurements, where the lack of any voids or cracks is remarked due to the improved crystallinity and the absence of defects in the films. Thus, as a result of the enhanced mobility, the resistivity of undoped and Cu doped CdTe thin films at room temperature decreased with the increase of Cu incorporation level from $66.38 \times 10^{-4} (\Omega \text{ cm})$ for CdTe: 0 wt% to $2.93 \times 10^{-4} (\Omega \text{ cm})$ for CdTe: 10 wt%. This is in accordance with the reported huge reductions in the electrical resistivity of CdTe single crystals [55–58] and thin films [59] upon the incorporated tiny amount of Cu. Thus, upon the increase of Cu^{2+} ions concentration instead of the Cd^{2+} ions concentration, more electrons (free carrier concentration) are promoted to the conduction band, resulting in a further decrease in resistivity. This explains the observed decrease in resistivity with increasing Cu content. In order to investigate the mechanism of conductivity, the temperature-dependent dc conductivity measurements (in the form of $\ln \sigma$ versus $1000/T$ representations) of nanocrystalline undoped and Cu-doped CdTe films with different Cu concentrations were analyzed and are presented in Fig. 8a. Obviously, a non-linear temperature-dependent conductivity behavior is observed. Further, it was observed that the electrical dc conductivity of nanocrystalline undoped and Cu-doped CdTe films increases exponentially with increasing temperature. As a consequence, the results

Fig. 6 **a** The spectral dependence of the refractive of pure and Cu-doped CdTe film with different Cu concentrations. **b** The spectral variation of k for Cu doped films with various Cu incorporation levels

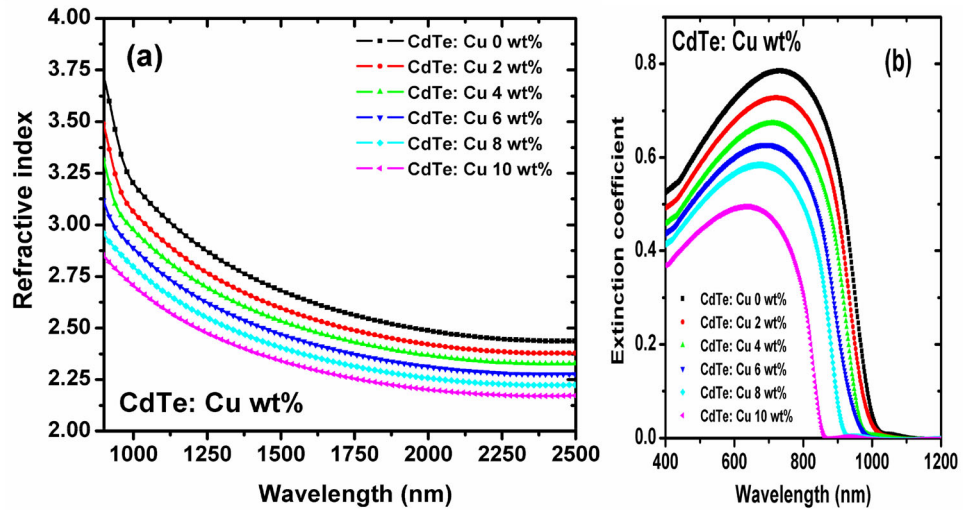


Fig. 7 The Hall mobility μ_H , carrier concentrations n_H , and resistivity ρ at room temperature of nanostructured undoped and Cu-doped CdTe film with various Cu incorporation levels

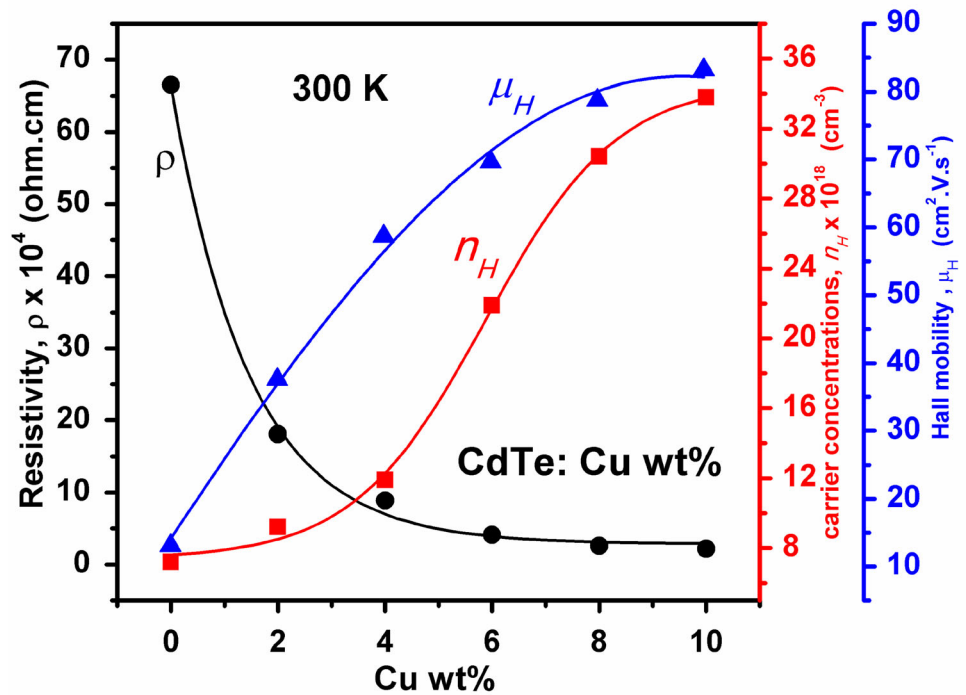


exhibit semiconducting-like behavior for all Cu-doped CdTe films over the entire measurement temperature region from 300 to 450 K. Additionally, the dc conductivity increases with the increase of the Cu incorporation level in the CdTe film which is attributed to the increase in the grain size, thereby reducing grain boundary scattering. Accordingly, it can be concluded that by increasing the Cu incorporation level in the CdTe film, as the conductivity increases, the performance of the CdTe layer in the

solar cell can be improved. Similar behavior has been reported for Cu doped CdSe films [60], Cu-doped CdTe films [27], and Ag–CdSe films [61]. Table 3 illustrates the decrease in the resistivity and the increase of the electrical conductivity at room temperature as the Cu content increases. Furthermore, according to the Arrhenius relationship $\sigma = \sigma_0 \exp(-E_a/kT)$, where E_a is the thermal activation energy and k is the Boltzmann constant, the results reveal two different regions with two slopes at low

and high distinct temperature ranges, which indicates two conduction mechanisms for the carrier transport in nanostructured undoped and Cu-doped CdTe films.

Consequently, the high-temperature activation energy (387–450 K) E_{a1} and low-temperature activation energy (300–386 K) E_{a2} of undoped and Cu-doped CdTe films are evaluated based on the slope of the curves in the two regions using the following equation: $\sigma = \sigma_1 \exp(-E_{a1}/kT) + \sigma_2 \exp(-E_{a2}/kT)$, where σ_1 and σ_2 are the pre-exponential factors. The values of E_{a1} and E_{a2} of undoped and Cu-doped CdTe films are summarized in Table 3. The low-temperature activation energy (E_{a2}) may be due to the low-temperature conductivity by hopping of carriers between the localized states above the edge of the valence band to the extended states in the conduction band, while in the high-temperature region, the normal type of band conduction in extended states can be considered to be the main mode of the conduction mechanism. On the other hand, it is found that the low-temperature activation energy E_{a2} decreases as the Cu content increases from 58 (CdTe: 0 wt%) to 25 meV (CdTe: 10 wt%). Also, the high-temperature activation energy E_{a1} is found to decrease with the increase of the Cu incorporation level from 578 (CdTe: 0 wt%) to 320 meV (CdTe: 10 wt%). The decrease in activation energy is attributed to the observed increase in crystallinity and decrease in defects. Different groups similarly reported a decrease in activation energy with increasing dopant concentration [62, 63]. Besides, at all temperatures up to room temperature, the dependence of $\ln \sigma$ and $T^{-1/4}$ in the undoped and Cu-doped CdTe nanostructure film is determined, which is an excellent tool for examining the hopping conduction mechanism, particularly the Mott's variable range hopping conduction model (VRH). It is worth mentioning that VRH in semiconductors is expected to dominate at appropriately low temperatures [60]. Therefore, the low-temperature dependence of the conductivity of undoped and Cu-doped CdTe nanostructured films can be analyzed based on Mott's variable range hopping conduction model (VRH) [64]:

$$\sigma T^{1/2} = \sigma_0 \exp\left(-\left(T_0/T\right)^{1/4}\right), \tag{5}$$

where Mott temperature T_0 is given by [65]

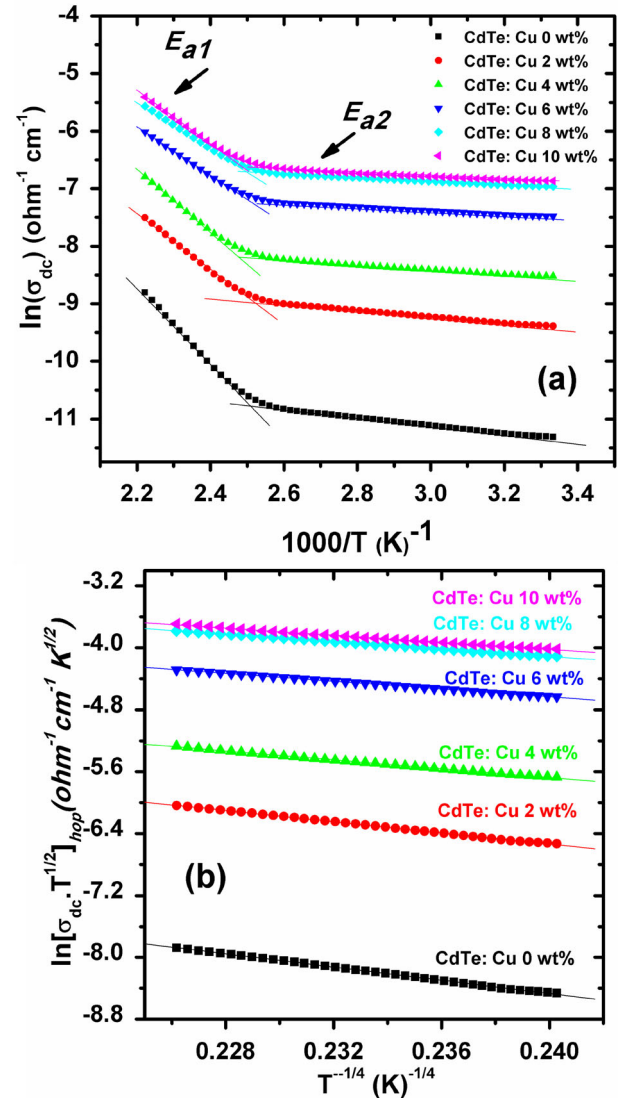


Fig. 8 **a** $\ln \sigma_{dc}$ versus $1000/T$ of undoped and Cu-doped CdTe nanostructure film with various Cu incorporation levels. **b** $\ln (\sigma_{dc} T^{1/2})$ versus $T^{-1/4}$ of undoped and Cu-doped CdTe nanostructure film with various Cu incorporation levels

$$T_0 = C_0 \left(\frac{\alpha^3}{kN(E_F)} \right), \tag{6}$$

where $N(E_F)$ is the density of states at the Fermi level, α is the exponential decay coefficient of the localized states wave function ($\approx 0.124 \text{ \AA}^{-1}$ [66]), and $C_0 (\approx 24/\pi)$ is the constant of proportionality. The observed linear low-temperature dependence of the conductivity in $\ln (\sigma T^{1/2})$ and $(T^{-1/4})$ represents the undoped and Cu-doped CdTe nanocrystalline films (see Fig. 8b), indicating a dominant variable range hopping (VRH) conduction mechanism where the

low-temperature conduction mechanism is ascribed to hopping of free carriers between localized states. Furthermore, the hopping distance R , the hopping energy W , and the density of states at the Fermi level $N(E_F)$ are calculated at room temperature (300 K) for undoped and Cu doped CdTe nanostructured films from the linear correlation slope shown in Fig. 8b and are summarized in Table 3 [60]. Apparently, as Cu incorporation increases from CdTe: 0 wt% to CdTe: 10 wt%, the density of state increases from $1.178 \times 10^{17} \text{ eV}^{-1} \text{ cm}^{-3}$ to $14.28 \times 10^{17} \text{ eV}^{-1} \text{ cm}^{-3}$. Also, it was found that the values of αR [734.51(CdTe: 0 wt%)–60.58 (CdTe: 10 wt%)] are > 1 and the values of W [0.053 (CdTe: 0 wt%)–0.029 (CdTe: 10 wt%)] are greater than the thermal energy (0.0259 eV), which are essential conditions for the above-mentioned factors to be consistent with the Mott's VRH [67, 68]. Finally, $\alpha R > 1$ indicates that the carriers are more localized in the trap states.

4 Summary

To summarize, pure and Cu-doped CdTe nanostructured thin films were deposited by electron beam evaporation technique on glass substrates. The XRD investigation shows that all the films are cubic zinc blende structure. It was found that as the Cu incorporation level increases from 0 to 10 wt%, the average crystallite size increases from 16 to 18 nm, while the microstrain decreases from $1.2 \times 10^{-3} \text{ (Lin m}^{-2}\text{)}$ to $0.70 \times 10^{-3} \text{ (Lin m}^{-2}\text{)}$. The average transmittance of Cu-doped CdTe films in the near-infrared region was found to vary from 78 to 82%, which can be used as an n-type window layer for photovoltaic solar cell applications. The optical band gap energy of Cu-doped CdTe films increases from 1.485 to 1.683 eV as the Cu concentration increases from 0 to 10 wt%. The optical analysis of the spectral behavior of the optical constants of Cu-doped CdTe films shows that the refractive index and extinction coefficient decrease with the increase of the Cu concentration in CdTe matrix. It is found that the resistivity decreases, while the dc electrical conductivity increases at room temperature with increasing Cu concentration. Additionally, it is observed that the temperature-dependent conductivity of nanostructured undoped and Cu-doped CdTe films shows two conduction mechanisms of the carrier transport. Mott's variable range hopping conduction mechanism model (VRH)

is used to interpret the low-temperature dependence of the conductivity, the behavior of hopping distance R , the hopping energy W , and the density of states at the Fermi level $N(E_F)$ of undoped and Cu-doped CdTe nanostructured films. Finally, p-type conduction behavior is observed from Hall effect measurements for all the films. Besides, the carrier concentration and Hall mobility increase with increasing Cu incorporation level. It can be concluded that as the Cu incorporation level increases, the conductivity increases, thereby improving the performance of the CdTe absorber layer in the solar cell structure.

Acknowledgements

The authors extend their appreciation to the Deputyship for Research & Innovation, Ministry of Education in Saudi Arabia for funding this research work through project Number 1527110410.

References

1. M.C. Schlamp, X.G. Peng, A.P. Alivisatos, *J. Appl. Phys.* **82**, 5837 (1997)
2. P.C. Sarmah, A. Rahman, Current-voltage characteristics of Ag, Al, Ni-(n) CdTe junctions. *Bull. Mater. Sci.* **24**(4), 411–414 (2001)
3. S.T. Sundari, V. Swaminathan, A.K. Tyagi, T. Mahalingam, Microstructural studies of oxygen irradiated CdTe thin films. *Phys. Status Solidi A* **177**(2), 495–502 (2000)
4. C. Polop, I. Mora-Sero, C. Munuera, J. Garcia de Andres, V. Munoz-Sanjose, C. Ocal, *Acta Mater.* **54**, 4285 (2006)
5. M. Niraula, K. Yasuda, T. Ishiguro, Y. Kawauchi, H. Morishita, Y. Agata, Metal-organic vapor-phase epitaxy growth and characterization of thick (100) CdTe layers on (100) GaAs and (100) GaAs/Si substrates. *J. Electron. Mater.* **32**(7), 728–732 (2003)
6. N. Lovergine, P. Prete, L. Tapfer, F. Marzo, A.M. Mancini, Hydrogen transport vapour growth and properties of thick CdTe epilayers for RT X-ray detector applications. *Cryst. Res. Technol.* **40**(10–11), 1018–1022 (2005)
7. P. Banerjee, R. Ganguly, B. Ghosh, *Appl. Surf. Sci.* **256**, 213 (2009)
8. K.M. Garadkar, S.J. Pawar, P.P. Hankare, A.A. Patil, *J. Alloys Compd.* **491**, 77 (2010)
9. F. de Moure-Flores, J.G. Quinones-Galvan, A. Guillen-Cervantes, J.S. Arias-Ceron, A. Hernandez-Hernandez, J. Santoyo-Salazar, J. Santos-Cruz, S.A. Mayen Hernandez, M.L.

- de la Olvera, J.G. Mendoza-Alvarez, M. Melendez-Lira, G. Contreras-Puente, *J. Cryst. Growth* **386**, 27 (2014)
10. V. Kosyak, A. Opanasyuk, P.M. Bukivskij, Yu.P. Gnatenko, *J. Cryst. Growth* **312**, 1726 (2010)
 11. R. Raj Singh, D. Painuly, R.K. Pandey, *Mater. Chem. Phys.* **116**, 261 (2009)
 12. E.R. Shaaban, N. Afify, A. El Taher, *J. Alloys Compd.* **482**, 400 (2009)
 13. K. Punitha, R. Sivakumar, C. Sanjeeviraja, V. Sathe, V. Ganesan, *J. Appl. Phys.* **116**, 213502 (2014)
 14. C. Doroody, K.S. Rahman, S.F. Abdullah, M.N. Harif, H.N. Rosly, S.K. Tiong, N. Amin, Temperature difference in close spaced sublimation (CSS) growth of CdTe thin film on ultrathin glass substrate. *Results Phys.* **18**, 103213 (2020)
 15. M.A. Islam, H. Misran, M. Akhtaruzzaman, N. Amin, Influence of oxygen on structural and optoelectronic properties of CdS thin film deposited by magnetron sputtering technique. *Chin. J. Phys.* **67**, 170–179 (2020)
 16. Z. Xie, Y. Sui, J. Buckeridge, C.R.A. Catlow, T.W. Keal, P. Sherwood, A. Walsh, M.R. Farrow, D.O. Scanlon, S.M. Woodley, A.A. Sokol, Donor and acceptor characteristics of native point defects in GaN. *J. Phys. D Appl. Phys.* **52**, 335104 (2019)
 17. B. Choudhury, M. Dey, A. Choudhury, Shallow and deep trap emission and luminescence quenching of TiO₂ nanoparticles on Cu doping. *Appl. Nanosci.* **4**, 499–506 (2014)
 18. S.L. Himanshu, A. Patel, M.D. Thakur, M.S. Kannan, Dhaka, Analysis of different annealing conditions on physical properties of Bi doped CdTe thin films for potential absorber layer in solar cells. *Sol. Energy* **199**, 772–781 (2020)
 19. O. Vigil-Galan, E. Sánchez-Meza, J. Sastre-Hernandez, F. Cruz-Gandarilla, E. Marin, G. Contreras-Puente, E. Saucedo, C.M. Ruiz, M. Tufino-Velázquez, A. Calderon, Study of the physical properties of Bi doped CdTe thin films deposited by close space vapour transport. *Thin Solid Films* **516**, 3818–3823 (2008)
 20. U. Alver, E. Bacaksiz, E. Yanmaz, Structural, magnetic and optical properties of Co-diffused CdTe thin films. *J. Alloys Compd.* **456**, 6–9 (2008)
 21. K.A. Aris, K.S. Rahman, A.M. Ali, B. Bais, I.B. Yahya, Md. Akhtaruzzaman, H. Misran, S.F. Abdullah, M.A. Alghoul, N. Amina, A comparative study on thermally and laser annealed copper and silver doped CdTe thin film solar cells. *Sol. Energy* **173**, 1–6 (2018)
 22. Sh.U. Yuldashev, Y.B. Hou, J.H. Leem, C.K. Kang, S.H. Park, T.W. Kang, T.W. Kim, Effects of hydrogenation and annealing on the shallow donor-band recombination in indoped CdTe epitaxial layers grown on p-CdTe (211) substrates. *J. Phys. Chem. Solids* **61**, 711–718 (2000)
 23. T. Manimozhi, T. Logu, J. Archana, M. Navaneethan, K. Sethuraman, K. Ramamurthi, Enhanced photo-response of CdTe thin film via Mo doping prepared using electron beam evaporation technique. *J. Mater. Sci. Mater. Elect.* **31**, 21059–21072 (2020)
 24. B. Monemar, E. Molva, L. Si Dang, *Phys. Rev. B* **33**, 1134 (1986)
 25. M. El-Hagary, S.H. Moustafa, H. Hashem, E.R. Shaaban, M. Emam-Ismael, Influences of Mn doping on the microstructural, semiconducting, and optoelectronic properties of HgO nanostructure films. *J. Am. Ceram. Soc.* **102**, 4737–4747 (2019)
 26. M.H. Cho, D.H. Ko, K. Jeong, S.W. Whangbo, C.N. Whang, S.J. Cho, Growth stage of crystalline Y₂O₃ film on Si(100) grown by an ionized cluster beam deposition. *J. Appl. Phys.* **85**, 2909–2914 (1999)
 27. M. Thangaraju, A. Jayaram, R. Kandasamy, Structural, morphological, optical and electrical properties of e-beam deposited nanocrystalline CdTe: Cu alloy thin films from mechanical alloyed samples. *Appl. Surf. Sci.* **449**(15), 2–9 (2018)
 28. M. Dehimi, T. Touam, A. Chelouche, F. Boudjouan, D. Djouadi, J. Solard, A. Fischer, A. Boudrioua, A. Doghmane, Effects of low Ag doping on physical and optical waveguide properties of highly oriented sol-gel ZnO thin films. *Adv. Condense. Matter Phys.* **2015**, 1–10 (2015)
 29. T. Saidani, M. Zaabat, M.S. Aida, B. Boudine, Effect of copper doping on the photocatalytic activity of ZnO thin films prepared by sol-gel method. *Superlattices Microstruct.* **88**, 315–322 (2015)
 30. M.I. Amer, S.H. Moustafa, M. El-Hagary, *Mater. Chem. Phys.* **248**, 122892 (2020)
 31. L. Ma, X. Ai, X. Wu, Effect of substrate and Zn doping on the structural, optical and electrical properties of CdS thin films prepared by CBD method. *J. Alloys Compd.* **691**, 399e406 (2017)
 32. J. Zhou, X. Wu, G. Teeter, B. To, Y. Yan, R. Dhere, T. Gessert, CBD Cd_{1-x}Zn_xS thin films and their application in CdTe solar cells. *Phys. Status Solidi (b)* **241**, 775778 (2004)
 33. N.E. Makori, I.A. Amatalo, P.M. Karimi, W.K. Njoroge, Optical and electrical properties of CdO: Sn thin films for solar cell applications. *Int. J. Optoelectron. Eng.* **4**(1), 11–15 (2014)
 34. S.H. Wemple, J.A. Seman, *Appl. Opt.* **12**, 2947 (1973)
 35. J. Tauc, in *Optical properties of solids*. ed. by F. Abeles (North-Holland, Amsterdam, 1969)
 36. E.A. Davis, N.F. Mott, *Philos. Mag.* **22**, 903 (1970)
 37. B.D. Viezbicke, S. Patel, B.E. Davis, D.P. Birnie III., *Phys. Status Solidi (b)* **252**, 1700–1710 (2015)

38. R. Kumeravel, S. Bhuvaneshwari, K. Ramamurthi, V. Krishnakumar, Structural, optical and electrical properties of molybdenum doped cadmium oxide thin films prepared by spray pyrolysis method. *Appl. Phys. A* **109**, 579–584 (2012)
 39. G. Jellison Jr., F. Modine, *Appl. Phys. Lett.* **69**, 371–373 (1996)
 40. S. Jena, R.B. Tokas, S. Thakur, D.V. Udupa, *Optik* **185**, 71–81 (2019)
 41. D. Minkov, *J. Phys. D Appl. Phys.* **22**, 1157 (1989)
 42. J. Gonzalez-Leal, E. Marquez, A. Bernal-Oliva, J. Ruiz-Perez, R. Jimenez-Garay, *Thin Solid Films* **317**, 223–227 (1998)
 43. M. Emam-Ismael, M. El-Hagary, E.R. Shaaban, S. Althoyaib, *J. Alloys Compd.* **529**, 113–121 (2012)
 44. M. Emam-Ismael, E.R. Shaaban, M. El-Hagary, *J. Alloys Compd.* **663**, 20–29 (2016)
 45. R. Swanepoel, *J. Phys. E Sci. Instrum.* **16**, 1214 (1983)
 46. J.C. Manificier, J. Gasiot, J.P. Fillard, *J. Phys. E* **9**, 1002 (1976)
 47. M. El-Hagary, M. Emam-Ismael, E.R. Shaaban, Optical properties of glasses (TeO₂–GeO₂–K₂O) thin films co-doped with rare earth oxides Sm₂O₃/Yb₂O₃. *J. Alloys Compd.* **485**(1–2), 519–523 (2009)
 48. E.R. Shaaban, M. El-Hagary, M. Emam-Ismael, M.B. El-den, Optical band gap, refractive index dispersion and single-oscillator parameters of amorphous Se₇₀S_{30-x}Sb_x semiconductor thin films. *Philos. Mag.* **91**(12), 1679–1792 (2011)
 49. T. Moss, *Proc. Phys. Soc. Sect. B* **63**, 167 (1950)
 50. N.M. Ravindra, S. Auluck, V.K. Srivastava, *Phys. Status Solidi (b)* **93**, K155 (1979)
 51. P.J.L. Herve, L.K.J. Vandamme, *J. Appl. Phys.* **77**, 5476–5477 (1995)
 52. Elliott, *The Physics and Chemistry of Solids* (Wiley, Chichester, 2000).
 53. K. Senthil, D. Mangalaraj, S.K. Narayandass, S. Adachi, *Mater. Sci. Eng. B* **78**, 53–58 (2000)
 54. E.R. Shaaban, M. El-Hagary, M. Emam-Ismael, A.M. Abd Elnaeim, S.H. Moustafa, Optical characterization of polycrystalline ZnSe_{1-x}Te_x thin films using variable angle spectroscopic ellipsometry and spectrophotometry techniques. *Mater. Sci. Semicond. Process.* **39**, 735–741 (2015)
 55. E. Kučys, J. Jerhot, K. Bertulis, V. Bariss, *Phys. Status Solidi A* **59**(1), 91–99 (1980)
 56. K.K. Chin, T.A. Gessert, W. Su-Huai, *Paper Presented at the 35th IEEE Photovoltaic Specialists Conference (PVSC)* (Honolulu, Hawaii, 2010).
 57. J. Ma, S.H. Wei, T.A. Gessert, K.K. Chin, *Phys. Rev. B* **83**(24), 245207 (2011)
 58. B. Biglari, M. Samimi, M. Hage-Ali, J.M. Koebel, P. Siffert, *J. Cryst. Growth* **89**(4), 428–434 (1988)
 59. A. Ali, N.A. Shah, A.K.S. Aqili, A. Maqsood, Investigation of Cu-containing low resistivity CdTe thin films deposited by the two-source evaporation technique. *J. Semicond. Sci. Technol.* **21**, 1296–1302 (2006)
 60. K. Sharma, G.S. Saini, S.K. Tripathi, A comparative study of transport properties of copper doped cadmium selenide thin films at two dopant concentrations. *J. Mater. Sci. Mater. Electron.* **29**, 9596–9604 (2018)
 61. R. Sahebi, M.R. Roknabadi, M. Behdani, Effect of Ag-doping on the structural, optical, electrical and photovoltaic properties of thermally evaporated cadmium selenide thin films. *Mater. Res. Express* **6**, 126453 (2019)
 62. A.J. Al-Douri, F.Y. Al-Shakily, A.A. Alnajjar, M.F. Alias, The role of dopant concentration on conductivity and mobility of CdTe thin films. *Adv. Condens. Matter Phys.* (2011). <https://doi.org/10.1155/2011/910967>
 63. N.M. Megahid, M.M. Wakkad, E.K.H. Shokr, N.M. Abass, Microstructure and electrical conductivity of In doped CdS thin films. *Phys. B* **353**(3–4), 150–163 (2004)
 64. N.F. Mott, *J. Non-Cryst. Solids* **8**, 191 (1972)
 65. N.F. Mott, E.A. Davis, *Electronic Processes in Non-Crystalline Materials*, 2nd edn. (Clarendon, Oxford, 1979).
 66. S. Ramchandrarao, M. Nagabhooshanam, V. Hari Babu, *Cryst. Res. Technol.* **25**, 55 (2006)
 67. T.G. Abdel-Malik, R.M. Abdel-Latif, A. Sawaby, S.M. Ahmed, *J. Appl. Sci. Res.* **4**, 331 (2008)
 68. N.F. Mott, E.A. Davis, *Philos. Mag.* **22**, 903 (1970)
- Publisher's Note** Springer Nature remains neutral with regard to jurisdictional claims in published maps and institutional affiliations.